

Design of PSR with Different Feed Configurations and Partition Lens System for Skin Cancer Treatment

Petrishia Arockiasamy and Sasikala Mohan

Department of ECE, Anna University, Chennai, Tamilnadu, India
petrishia7@yahoo.com, sasikala@annauniv.edu

Abstract — The Prolate Spheroidal Impulse Radiating Antenna (PSIRA) focuses pulsed radiation in the near field with a small beam width allowing the application of non-invasive skin cancer treatment. In this proposed work, SWB (Slanted Wire Bicone), EPH (Elliptical Profile Horn), TSVS (Tapered Slot Vivaldi Shape) and Tapered Arm Conical Plate (TACP) feed antenna configurations for Prolate Spheroidal Reflector (PSR) are explored to enhance the spatial resolution on biological target. The feed antenna is placed at the first focal point and the target is located at the second focal point of the PSR. Next, the resolution of focused electric field on the target is enhanced by using near field focusing lens. A 3 layer partition lens system is placed before the target to reduce the spot size of the focused field on the target. The delivery of subnanosecond pulses using reflector in conjunction with and without partition lens system on the biological target is compared for all feed antenna configurations. Tapered Arm Conical Plate (TACP) fed PSR with the 3 layer partition lens system greatly reduces the spot size to 0.5 cm along lateral direction and 1 cm along axial direction. The enhancement in spatial resolution is much favorable to reduce the damage of healthy tissues during cancer treatment.

Index Terms — Near field focusing lens, non-invasive cancer treatment, prolate spheroidal impulse radiating antenna, subnanosecond electric pulse, ultra wide band antenna.

I. INTRODUCTION

Recent research shows that fast, intense electromagnetic pulses can be used to kill melanoma cells [1, 2]. The conventional treatment for melanoma is an invasive method which delivers electric pulses in nanosecond range using electrodes into the skin. The non-invasive technique involves PSIRA to deliver an electric pulse. The non-invasive treatment limits surgery, reduces the pain, scarring and mortality of the patients while remaining cost effective and safe. From the past researches, it is observed that if an intense electric field is applied to cancer cells, it introduces a programmed cell death called apoptosis [3].

Xiao et al. showcased the high power electromagnetic pulses can treat melanoma cells [4, 5]. The intense pulses with subnanosecond range is preferred to obtain the higher probability of penetration into the interior of the cells. The preferred duration of subnanosecond pulse is in the range of 100-200 ps making it possible to focus the radiation on the target efficiently and produce small spot size on the target. Baum et al. designed PSIRA to deliver subnanosecond pulse. The PSIRA acts as a high power radiation source for melanoma treatment [6]. The PSIRA is based on the two foci of an ellipse. It radiates subnanosecond intense pulses from the first focus to the second focus. The feed of the PSIRA is an ultra-wideband antenna. The spatial resolution on the target is enhanced by placing lens system before the target. Kumar et al. designed a graded index lens system which is located before the dielectric slab ($\epsilon_r = 9$). The spot diameter obtained from the numerical simulation is 1.187 cm [7].

In the proposed work, four types of PSIRA with partition lens are designed and their performance is compared in terms of spatial resolution on the target.

This paper is organized as follows. Section II presents the design of PSR. In Section III, the different feed configuration for PSR is discussed. Section IV discusses the partition lens system design. The skin model is presented in Section V. Section VI presents the comparative results of the numerical simulations of the PSIRA and focusing lens system.

II. PROLATE SPHEROIDAL REFLECTOR DESIGN

The Impulse Radiating Antenna (IRA) is a class of focused aperture antennas that have been used extensively for the generation and radiation of ultra wide band electromagnetic pulses [8, 9]. The IRA can effectively focus its radiation in the near field by using Prolate Spheroidal Reflector (PSR). A fast rising transient pulse is propagated from the first focus of the PSR. The wave is then refocused on the second focus of the PSR to obtain a very narrow impulsive waveform.

The PSIRA consists of two main parts, feed arms and a reflector. The schematic diagram of Prolate

Spheroidal Reflector is shown in Fig. 1. PSR is an elliptical reflector. It has two focal points. The feed antenna is placed at the first focal point. The target (skin) is placed at the second focal point. The radiated electromagnetic wave from the first focal point is concentrated at the second focal point where the target is placed. PSR is designed using the reflector geometry proposed by Xiao et al. [6]. The semi major axis (a) of the reflector is 29.8 cm. The semi minor axis (b) is 25 cm. It has two foci. The focal distance $z_0 = \sqrt{a^2 - b^2}$, i.e., 16.3 cm. The second focal point is closer to the near field region with focal distance less than $2D^2/\lambda$, where D is aperture diameter and λ is the wavelength. The distance between the two focal point is 32.6 cm.

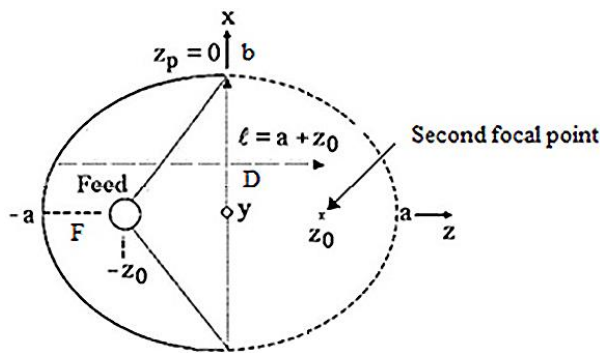


Fig. 1. Schematic diagram of prolate spheroidal reflector with geometrical parameter.

III. DESIGN OF FEED ANTENNA CONFIGURATIONS OF PSR

The radiation characteristics of IRA at high frequencies are very sensitive to the design of feeding structure. The design of different feed antenna structures for PSR is presented in this section.

A. Slanted Wire Bicone (SWB) fed PSR

The Slanted Wire Bicone (SWB) fed PSIRA design is presented. It is much suitable for ultra wide band application such as intense subnanosecond pulse radiation. The design of SWB is derived from bicone antenna [10]. The radiation is focused in one direction by slanting the two cones in the desired direction by the angle of 30° , which is shown in Fig. 2 (a). In order to construct a light weight feed structure, the wire bicone is chosen instead of solid structure. The inner diameter of conical structure is 2 cm and the outer diameter is 22 cm. The excitation gap between the cone is optimized to 1 cm. The entire simulation setup is shown in Fig. 2 (b).

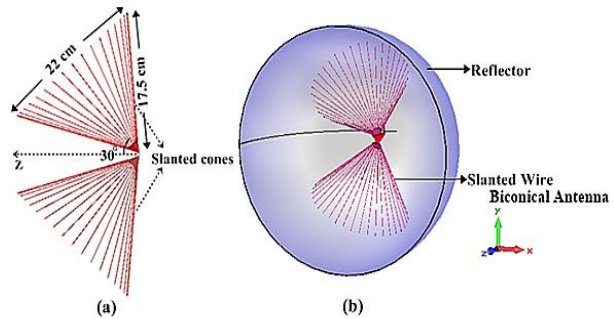


Fig. 2. SWB fed PSR: (a) geometry of SWB feed and (b) simulation model of SWB fed PSR.

B. Elliptical Profile Horn (EPH) fed PSR

The design of Elliptical Profile Horn (EPH) feed for PSR is presented. The EPH feed is simple and is designed from the single quadrant of the elliptical profile, which is shown in Fig. 3 (a). In this work the longitudinal section of the ellipse in the $y-z$ plane is chosen, because it is easy to bend the surface smoothly at both the low impedance (driving point) as well as free space ends of the horn [11].

Two significant variables in the design of the elliptical profile horn are overall length a (semi major axis of the ellipse) and the height h (separation between the plate which is determined from the semi minor axis (b)).

The coordinates of the ellipse can be obtained from:

$$\frac{x^2}{a^2} + \frac{(y-h)^2}{b^2} = 1. \tag{1}$$

The parameter m is given by:

$$m = e^2 = 1 - \frac{b^2}{a^2}, \tag{2}$$

e -eccentricity of the ellipse.

The length of the arc described by the ellipse is given by $E(m)$, the complete elliptic integral of the first kind,

$$E(m) = \int_0^{\pi/2} \sqrt{1 - m \sin^2 \theta} d\theta. \tag{3}$$

The simulation setup is shown in Fig. 3 (b). The semi major axis (a) of elliptic profile is 15 cm and semi minor axis (b) is 16 cm. At the excitation point the spacing between the plates is properly designed in order to avoid the higher order modes. For the design of horn structure the higher order modes are undesirable. So the feed gap has to be less than the wavelength at the highest operating frequency. The edges of the plates are tapered. The curvature of the tapering is optimized to completely remove the fluctuations in the main lobe at higher frequencies.

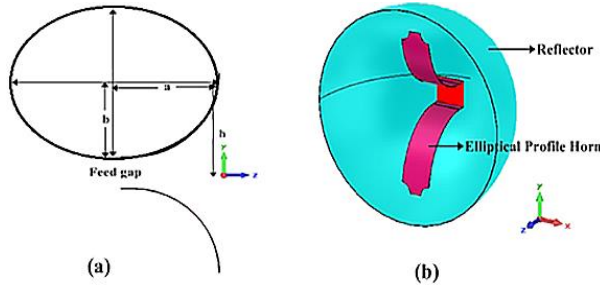


Fig. 3. EPH fed PSR: (a) geometry of elliptical profile and (b) simulation model of EPH fed PSR.

C. Tapered Slot Vivaldi Shaped (TSVS) fed PSR

The traditional Vivaldi feed arm structure for parabolic reflector has a low reflection loss in the entire frequency band but low radiation efficiency. The Tapered Slot Vivaldi Shaped (TSVS) feed arm shown in Fig. 4 (a) is designed in order to improve the radiation characteristics of the PSIRA. The Prolate Spheroidal Reflector with Tapered Slot Vivaldi Shaped feed arm is shown in Fig. 4 (b). It consists of two pairs of feed arms. The feed arms are separated by the arm angle $\varphi=70^\circ$ from the horizontal axis. The optimized arm angle ($\varphi=70^\circ$) is used because the antenna has uniform aperture field distribution in the entire frequency band of interest [12].

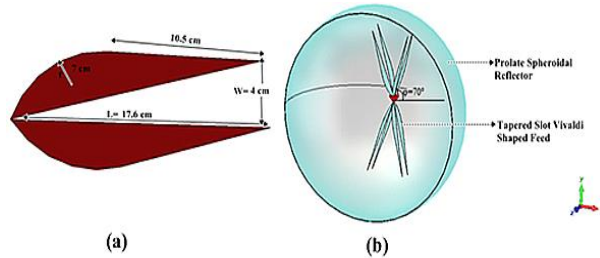


Fig. 4. TSVS fed PSR: (a) geometrical dimensions of TSVS feed and (b) simulation model of PSR with TSVS feed arms.

The TSVS feed is a combination of Vivaldi antenna and TEM coplanar transmission line. The Vivaldi shape is obtained by blending the edge of the coplanar transmission line with the radius(r) of 7 cm. The rounded portion of the TSVS feed is optimized to reduce the current reflection from the end of the antenna and to improve the radiation of low frequencies.

Two parts of the Vivaldi shape are joined at one end of the arm and the other end of the arm is arranged in such a way that it looks like a linearly tapered slot. The length of the slot, $L=17.6$ cm. The width of the tapered slot, $W=4$ cm. The thickness of the arm is considered as

1 mm. The pair of two feed arms is placed at the first focal point of the PSR. The upper and lower feed arms are separated by the optimized feed gap of 1 cm.

D. Tapered Arm Conical Plate (TACP) fed PSR

The TACP fed PSR is constructed with a diameter of 50 cm and four tapered conical plate feed arm with separation angle of $\varphi_o = 60^\circ$. The design of a conical structure mainly depends on the three angles β_0 , β_1 , and β_2 . The center angle is β_0 , and β_1 and β_2 are the lower and upper side angle of the feed arm, which is shown in Fig. 5 (a). The conically symmetric TEM feeding structure parameters [β_0 , β_1 , β_2] are related to the equivalent longitudinally symmetric structure parameters (semi major axis a , semi minor axis b , diameter D , focal length F).

The center angle is specified as β_0 :

$$\beta_0 = \arctan \left(1 / \left(\frac{2F}{D} - \frac{D}{8F} \right) \right), \quad (4)$$

$$\beta_1 = 2 \arctan \left(m^{1/4} \tan (\beta_0 / 2) \right), \quad (5)$$

$$\beta_2 = 2 \arctan \left(m^{1/4} \tan (\beta_1 / 2) \right), \quad (6)$$

β_1 and β_2 are the lower and upper side angle of the feed arm.

Figure 5 (b) shows the PSIRA with TACP feed. These arms are terminated by 200 Ω load which are used as a low frequency matching circuit. Different termination loads have been tried [13] and it has been observed that there is no resistive termination load that can match the feeding arms with the reflector to remove the standing waves. It means that there is some stored energy around the arm-reflector junction. Because of that stored energy at the junction, the observed impedance is a complex value. It is not easy to match the feeding arms with the reflector for the entire frequency band. In order to reduce the energy stored around the junction of the arm-reflector and to improve the gain of the IRA, the end part of the feeding arms are tapered.

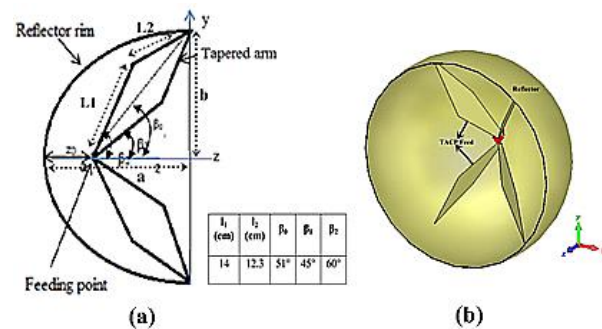


Fig. 5. TACP fed PSR: (a) configuration of TACP fed PSR and (b) simulation model of PSR with TACP feed arms.

E. Impedance and radiation characteristics of different feed configurations

The impedance and radiation characteristics of different feed configurations are presented. The spot size is one of the most important parameters to be considered for non-invasive cancer treatment. The spot is measured from the focal waveform at half power points.

The return loss and VSWR are calculated from Figs. 6 (a) and 7 (a) for SWB fed PSR. The return loss is -10 dB for the bandwidth of 600 MHz to 10 GHz. Within the band of 600 MHz to 10 GHz, the VSWR is lower than 2. The radiated pulse is focused to the second focal point where the target (skin) is placed. The focal waveform is shown in Fig. 8 (a). The maximum electric field measured is 49 V/m. The Full Width Half Maximum (FWHM) is 65ps.

The impedance characteristics of EPH fed PSIRA are shown in Figs. 6 (b) and 7 (b). The return loss is -10 dB for the bandwidth of 430 MHz to 15 GHz. The maximum electric field near second focus is measured as 100 V/m. The focal wave form is shifted towards the aperture of the reflector which is shown in Fig. 8 (b). The FWHM calculated from the focal waveform is 60 ps.

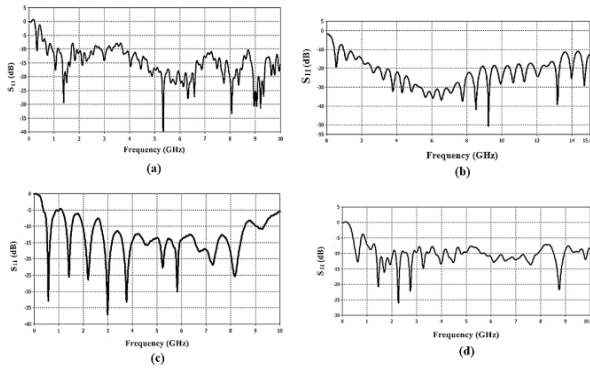


Fig. 6. Reflection parameter for: (a) SWB fed PSR, (b) EPH fed PSR, (c) TSVS fed PSR, and (d) TACP fed PSR.

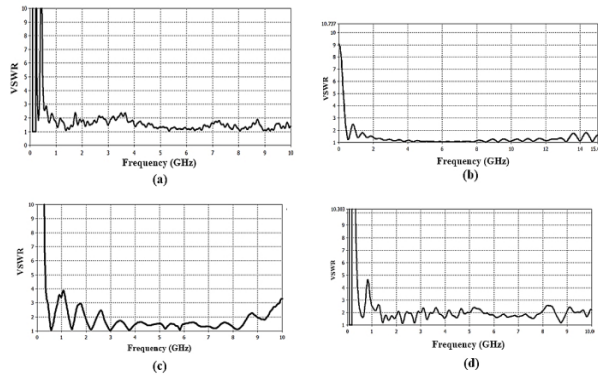


Fig. 7. VSWR for: (a) SWB fed PSR, (b) EPH fed PSR, (c) TSVS fed PSR, and (d) TACP fed PSR.

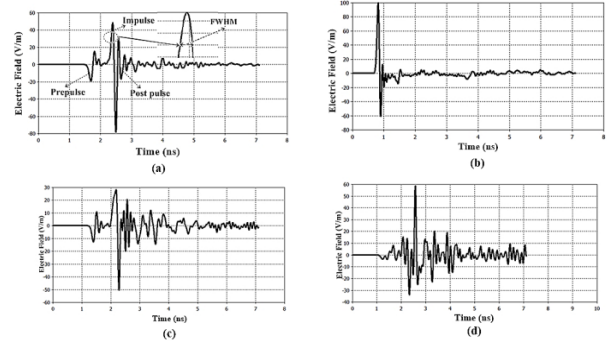


Fig. 8. Electric field at second focus in with an input Gaussian pulse. (a) SWB fed PSR, (b) EPH fed PSR, (c) TSVS fed PSR, and (d) TACP fed PSR.

In TSVS fed PSR, the return loss measured is -10 dB for the bandwidth of 500 MHz to 10 GHz from Fig. 6 (c). The return loss of -5 dB is obtained for the spectrum of 350 MHz to 10 GHz. Within the band of 500 MHz to 9.5 GHz, the VSWR is lower than 2 which is better than the case of traditional IRA, which is shown in Fig. 7 (c). The spot size measured from the focal wave form (Fig. 8 (c)) is 90ps.

The return loss and VSWR are measured from Figs. 6 (d) and 7 (d) for TACP fed PSR. The feed arm is well matched for the bandwidth of 1.5 GHz to 10 GHz. The FWHM measured from focal waveform Fig. 8 (d) is 100ps, which is the same as the rise time of the input signal.

IV. DESIGN OF PARTITION LENS

The design of the 3 layer partition lens is presented. The fast and intense electromagnetic pulse is illuminated to the target (skin) which is located at the second focal point. The major problem for concentrating the fields at the second focal point is the reflection. The dielectric property of the target medium and the medium though, which the incident wave propagates are different which causes reflections. The partition lens is used to focus the field at the second focal point. The addition of partition lens before the target leads to better match the wave to the target. The larger electric field and reduced spot size are obtained.

A. Partition lens design

The design of a partition dielectric lens is shown in Fig. 9. The partition lens is designed based on Fermat's Aplanatic principle and Fresnel law of refraction [14, 15]. The design contour of each layer is determined from the following equation:

$$y_i = f_i(x) = \sqrt{(n^2 - 1)x^2 - 2n(n - 1)Fx + (n - 1)^2F^2}, \quad (7)$$

where n is the refractive index of the lens, F is the focal length.

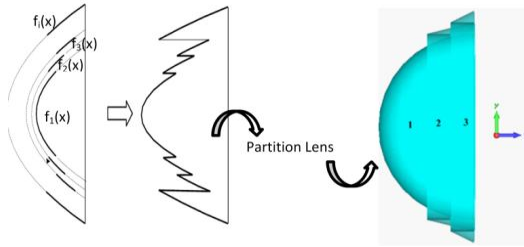


Fig. 9. Design of partition lens from hemisphere dielectric lens.

The thickness of the lens is varied from t_i to t_1 . The relative dielectric constant $\epsilon_r = 2$ for all three layers. In the lens design the phase difference between the electromagnetic waves plays an important role. The layers of the lens are designed with different focal length and different optical path. The electromagnetic waves through different parts of the lens have different phase. The partition lens is designed such that the phase difference between the electromagnetic waves through the different parts of the lens is an integer multiple of 2π till they arrive at the focal point.

L_i is the optical path of electromagnetic waves through the part of the lens,

$$\text{where } L_i = F_i + n \times t_i, \quad (8)$$

$F_i + t_i = \text{Constant}$, n is the refractive index of the lens, F_i is the focal length of the i^{th} layer, $t_i = \text{thickness of the } i^{\text{th}}$ layer.

The appropriate focal length for each layer is chosen to make sure that the difference of optical length between each layer is an integer multiple of the wavelength (3 cm). The design parameters are shown in Table 1 for 3 layers. The inner and outer radius is used to decide the area of each layer. This will have an effect on the focusing ability of the partition lens. The area of the partition is optimised in order to obtain reduced spot size and enhanced electric field at the second focus. The intensity of the wave decreases from the reflector and increases at the geometric focus. Adding partition lens allows one to increase the field intensity near the geometric focus, but the strongest intensity is still found along the axis and increases as the wave penetrates deeper into the tissue.

The proposed lens is used to solve the thickness and volume problem of the short focus dielectric lens. The field at the second focus is higher because the phase difference between electromagnetic waves through the different part of the lens is chosen as integer multiples of 2π .

Table 1: Design parameter for partition lens

Parameter	Layer-1	Layer-2	Layer-3
Dielectric constant (ϵ_r)	2	2	2
Focal length (cm)	9	6	3
Outer radius (cm)	12	13.5	15
Inner radius (cm)	0	12	13.5

V. SKIN MODEL DESCRIPTION

A. Two layer skin model

The skin model chosen in this case has been simulated with a specific length and width. This is a two layer model which consists of the epidermis and dermis with the thickness of 0.15 mm and 3.85 mm respectively. The length and width of the model have been specified by 5 cm x 5 cm. The 100 ps pulse (microwave frequency) is radiated from the PSIRA to the skin. The dielectric constant chosen for the skin model is 38 for our simulation.

The skin model is kept at the distance of 48.6 cm from the antenna vertex. The skin is modeled according to the dielectric properties given in Table 2 [16-22].

Table 2: Dielectric properties of skin model

Properties	Skin
Dielectric constant	38
Conductivity (S/m)	0.2
Material density (Kg/m^3)	1100
Thermal conductivity (W/K/m)	0.5
Heat capacity (KJ/K/kg)	3.35

VI. NUMERICAL SIMULATIONS AND DISCUSSION

A. Electromagnetic simulation

The entire simulation setup is shown in Figs. 10-13. The CST Microwave Studio, 3-D Finite Integration Time Domain (FITD), commercially available software is used for simulation. The CST Microwave Studio is a module in CST which is dedicated to fast and very accurate electromagnetic simulations of high frequency problems. This module contains different solvers for simulations of structures, both in time and frequency domain. The CST transient solver is suitable for wide band antenna simulations and electrically large structures. The simulation code is computed using CST transient solver. The PSIRA with the partition lens system and skin model for four types of configuration is shown in Figs. 10-13. The three layer focusing lens has its center at the second focal point. The radius and focal length is obtained from Table 1. The two layer skin model is used as target medium. The reflector and feed arms are assumed to be perfect electric conductors, the focusing lens and skin model are assumed to be lossless and dispersion less. The PSIRA is fed with the input of 1 V, 100ps rise time Gaussian signal.

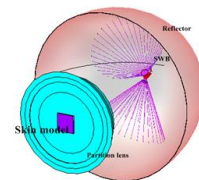


Fig. 10. Simulation design of SWB fed PSIRA with partition lens system and skin model.

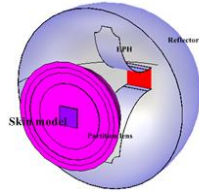


Fig. 11. Simulation structure of EPH fed PSIRA with partition lens system and skin model.

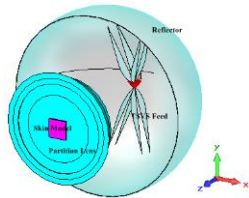


Fig. 12. Simulation setup of TSVS fed PSIRA with partition lens system and skin model.

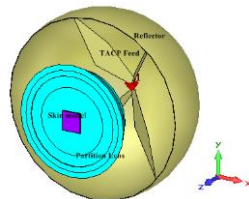


Fig. 13. Simulation design of TACP fed PSIRA with partition lens system and skin model.

B. Comparative spot size analysis

The spot size of the radiated pulse at the second focus plays a vital role in the treatment of skin cancer. The enhanced spatial resolution on the target reduces the damage of healthy tissue. The electric field component that contributes mostly to the electric field at the second focal point is the Y component. The amplitude of the electric field along X and Z directions are negligible. The electric field distribution is measured around the second focal point by placing the probe at regular spacing where the target is located.

This section presents the numerical simulation results of different feed antenna configurations for PSR with focusing lens. The electric field distribution is measured along lateral as well axial direction. The FWHM is obtained from the electric field distribution curve which is shown in Figs. 14-17 for all feed configurations. The beam width of the radiated electric field with and without lens is compared. The field intensity is maximum at the focal point and it is reduced to 50% with $\pm 1\text{ cm}$ near the focus for SWB, and TSVS fed PSR. In EPH fed PSR without lens configuration, the radiated impulse is not exactly focused on the second focal point. The peak of the impulse electric field on the

z axis is shifted slightly from the geometric focus towards the reflector, which is observed in the modeled result (Fig. 15 (a)). This is because the impulse decreases inversely with the distance while it is focused in space. At the focal point, even though coherent combinations of waves are obtained, the impulse electric field is still smaller than the nearby locations toward the reflector due to a large impulse width, $c\delta$ (in spatial units). In order that the maximum impulse amplitude occurs at the geometric focus, the impulse width needs to be small compared to both $2Z_0$ and $2b$ (similar discussion in the frequency domain can be seen in [23]). This shift of the impulse electric field is overcome by using partition lens. A pulse with faster rise time is allowed the shift of the focal spot towards the geometric focus. In TACP fed PSR maximum field intensity is obtained at the second focal point and it is reduced to 50% within $\pm 0.25\text{ cm}$ near the focal point.

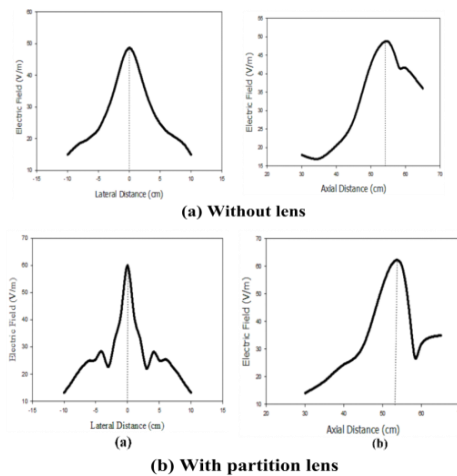


Fig. 14. Electric field distribution of SWB fed PSR at the second focal point: (a) without lens and (b) with partition lens.

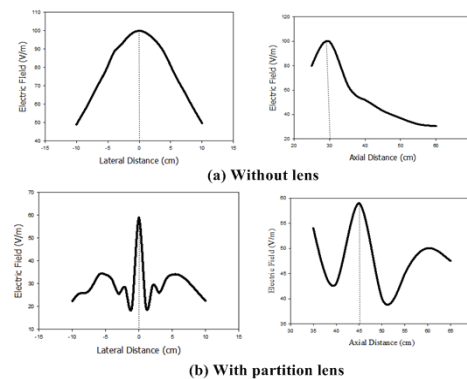


Fig. 15. Electric field distribution of EPH fed PSR at the second focal point: (a) without lens and (b) with partition lens.

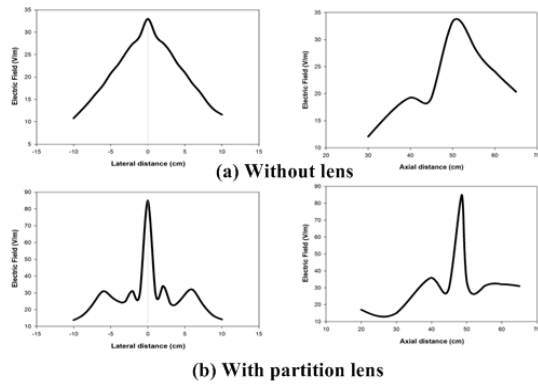


Fig. 16. Electric field distribution of TSVS fed PSR at the second focal point: (a) without lens and (b) with partition lens

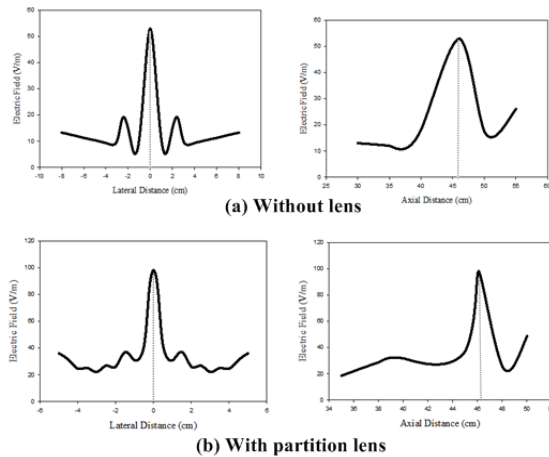


Fig. 17. Electric field distribution of TACP fed PSR at the second focal point: (a) without lens and (b) with partition lens.

Table 3 summarizes the radiation characteristics of all types of radiators. Their performance is compared in terms of electric field and spot size on the target.

The reflector dimension is the same for all configurations of PSIRA. The peak electric field for all feed configurations is compared. The TACP fed PSR provides the maximum electric field of 98 V/m. The spot diameter for TACP fed PSR with partition lens is less compared to the rest of the proposed PSIRAs. The spot size is measured from FWHM of electric field distribution around the second focal point along lateral and axial direction and shown in Figs. 18 (a) and 18 (b). It is observed that the spot size of TACP fed PSR is 1 cm along the lateral direction and 5 cm along the axial direction which is less compared to all configurations and it is further reduced to 0.5 cm along lateral direction and 1 cm along axial direction by using partition lens.

Table 3: Comparison of all types of PSIRA with and without partition lens system

Parameter	SWB Fed PSIRA	EPH Fed PSIRA	TSVS Fed PSIRA	TACP Fed PSIRA	SWB Fed PSIRA	EPH Fed PSIRA	TSVS Fed PSIRA	TACP Fed PSIRA
	Without Lens				With Partition Lens			
Reflector diameter (cm)	50	50	50	50	50	50	50	50
F/D	0.33	0.33	0.33	0.33	0.33	0.33	0.33	0.33
No. of arms	-	-	4	4	-	-	4	4
Separation between arms	-	-	70°	60°	-	-	70°	60°
Input Impedance (Ω)	100	100	200	200	100	100	200	200
Electric Field (V/m)	49	42	30	59.2	60	59	85	98
Spot size FWHM axial & FWHM lateral	Axial (cm)				Axial (cm)			
	10	13	14	5	8	7	2.5	1
	Lateral (cm)				Lateral (cm)			
	5	7.5	8	1	2	1	0.75	0.5

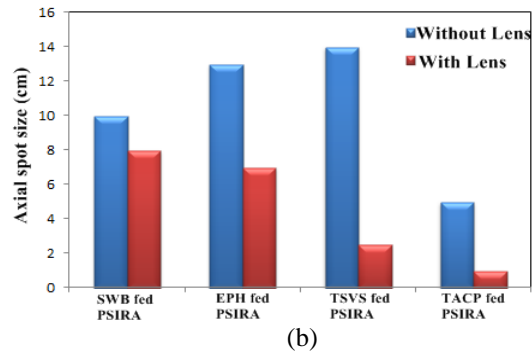
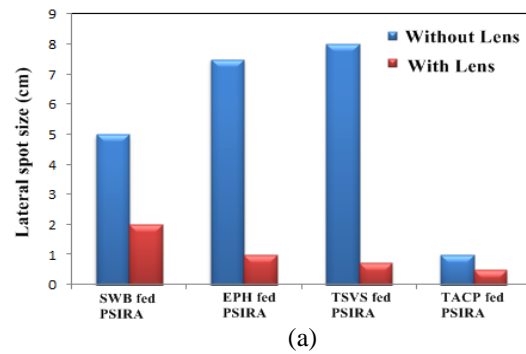


Fig. 18. (a) Spot size of all PSIRA with and without lens along lateral direction. (b) Spot size of all PSIRA with and without lens along axial direction.

VII. CONCLUSION

The Prolate Spheroidal Reflector (PSR) with different feed antenna configurations are designed to delivered subnanosecond pulses for non-invasive skin

cancer treatment. The 100ps electric pulse is launched from the feed antenna and is focused at the second focal point where the target is placed. Further, deep near field focusing is obtained using partition lens. The lens modifies the electric field distribution on the target along lateral as well as axial direction. The radiation characteristics of all PSIRA configurations with and without lens system are compared. The TACP fed PSR with partition lens system produces narrow spot size of 0.5 cm along lateral direction and 1 cm along axial direction. The enhanced resolution is obtained on the target using TACP fed PSR with partition lens system. Adding a dielectric lens allows one to increase the field intensity near the geometric focus which is more beneficial to reduce the input voltage requirement to obtain high electric field and to enhance the spatial resolution for the treatment of skin cancer.

REFERENCES

- [1] K. H. Schoenbach, B. Hargrave, R. P. Joshi, J. F. Kolb, R. Nuccitelli, C. Osgood, A. Pakhomov, M. Stacey, R. J. Swanson, J. A. White, S. Xiao, J. Zhang, S. J. Beebe, P. F. Blackmore, and E. S. Buescher, "Bioelectric effects of intense nanosecond pulses," *IEEE Trans. Dielectr. Electr. Insul.*, vol. 14, no. 5, pp. 1088-1119, Oct. 2007.
- [2] K. H. Schoenbach, S. Xiao, R. P. Joshi, J. T. Camp, T. Heeren, J. F. Kolb, and S. J. Beebe, "The effect of intense subnanosecond electrical pulses on biological cells," *IEEE Trans. Plasma Sci.*, vol. 36, no. 2, pp. 414-422, Apr. 2008.
- [3] R. Nuccitelli, U. Pliquett, X. Chen, W. Ford, J. Swanson, S. J. Beebe, J. F. Kolb, and K. H. Schoenbach, "Nanosecond pulsed electric fields cause melanomas to self-destruct," *Biochem. Biophys. Res. Commun.*, vol. 343, no. 2, pp. 351-360, May 2006.
- [4] S. Xiao, S. Guo, V. Nesin, R. Heller, and K. H. Schoenbach, "Subnanosecond electric pulses cause membrane permeabilization and cell death," *IEEE Transactions on Biomedical Engineering*, vol. 58, no. 5, May 2011.
- [5] S. Xiao, S. Guo, J. T. Camp, N. Vasyl, A. Pakhomov, R. Heller, and K. H. Schoenbach, "Biological cells response to high power electromagnetic Ppulses," *Frank Reidy Research Center For Bioelectrics*.
- [6] S. Xiao, S. Altunc, P. Kumar, C. E. Baum, and K. H. Schoenbach, "A reflector antenna for focusing in the near field," *IEEE Antennas Wireless Propag. Lett.*, vol. 9, pp. 12-15, 2010.
- [7] P. Kumar, S. Altunc, C. E. Baum, C. G. Christodoulou, E. Schamiloglu, and C. J. Buchenauer, "Radially inhomogeneous spherical dielectric lens for matching 100ps pulses into biological targets," *IEEE Trans. Plasma Sci. (Special Issue)*, vol. 38, no. 8, pp. 1915-1927, Aug. 2010.
- [8] K. H. Schonebach, S. Xiao, J. T. Camp, M. Migliaccio, S. J. Beebe, and C. E. Baum "Wideband, high-amplitude, pulsed antenna for medical therapies and medical imaging," *International Conference on Electromagnetics in Advanced Applications*, Torino, Sept. 14-18, 2009.
- [9] P. Kumar, S. Altunc, C. E. Baum, C. G. Christodoulou, and E. Schamiloglu, "Launching a fast (100 ps), high-voltage (> 100 kV) pulse into a biological target," *International Conference on Electromagnetics in Advanced Applications (ICEAA)*, Sydney, Australia, Sept. 2010.
- [10] N. Liu, Z. Zhang, G. Fu, Q. Liu, and L. Wang, "A compact biconical antenna for ultrawideband Applications," *IEEE 5th International Symposium on Microwave, Antenna, Propagation and EMC Technologies for Wireless Communications (MAPE)*, Chengdu, 2013.
- [11] J. A. G Malherbe and N. Barnes, "Tem horn antenna with an elliptic profile," *Microwave and Optical Technology Letters*, vol. 49, no. 7, July 2007.
- [12] M. Manteghi and Y. Rahmat Samii, "Improved feeding structures to enhance the performance of the reflector impulse radiating antenna (IRA)," *IEEE Transaction on Antenna and Propagation*, vol. 54, no. 3, pp. 823-834, Mar. 2006.
- [13] J. S. Tyo, "Optimization of the TEM feed structure for four-arm reflector impulse radiating antennas," *IEEE Trans. Antennas Propag.*, vol. 49, no. 4, pp. 607-614, Apr. 2001.
- [14] B. Nábělek, M. Malý, and V. Jirka, "Linear Fresnel lenses, their design and use," *Renewable Energy*, vol. 1, iss. 3-4, pp. 403-40, 1991.
- [15] *Geometrical Optics: Lens, Snell's Law, Fresnel Equations, Fermat's Principle, Refraction, Total Internal Reflection, Depth of Field*, General Books.
- [16] N. Chahat, M. Zhadobov, R. Sauleau, and S. I. Alekseev, "New method for determining dielectric properties of skin and phantoms at millimeter waves based on heating kinetics," *IEEE Transactions on Microwave Theory and Techniques*, vol. 60, no. 3, Mar. 2012.
- [17] J. T. Camp, Y. Jing, J. Zhuang, J. F. Kolb, S. J. Beebe, J. Song, R. P. Joshi, S. Xiao, and K. H. Schoenbach, "Cell death induced by subnanosecond pulsed electric fields at elevated temperatures," in *IEEE Transactions on Plasma Science*, vol. 40, no. 10, Oct. 2012.
- [18] Italian National Research Council-Institute for Applied Physics-Online. <http://niremf.ifac.cnr.it/tissprop/>
- [19] F. Gustrau and A. Bahr, "W-band investigation of material parameters, SAR distribution, and thermal

- response in human tissue,” *IEEE Transaction on Microwave Theory and Techniques*, vol. 50, no. 10, Oct. 2002.
- [20] E. B. Garon, D. Saucer, P. T. Vernier, T. Tang, Y. Sun, L. Marcu, M. A. Gundersen, and H. P. Koeffler, “In vitro and in vivo evaluation and a case report of intense nanosecond pulsed electric field as a local therapy for human malignancies,” *Int. J. Cancer*, vol. 121, no. 3, pp. 675-682, Aug. 2007.
- [21] C. Gabriel, S. Gabriel, and E. Corthout, “The dielectric properties of biological tissues: I. Literature survey,” *Physic. Med. Biol.*, vol. 41, pp. 2231-2249, 1996.
- [22] A. Peyman, S. Holden, and C. Gabriel, “Dielectric properties at microwave frequencies,” *RUM-3, ‘Mobile Telecommunications and Health Research Programme’*, 2009.
- [23] J. W. Sherman, III, “Properties of focused apertures in the Fresnel region,” *IRE Trans. Antennas Propag.*, vol. AP-10, no. 4, pp. 399-408, July 1962.